Microsyst Technol (2007) 14:69–78
DOI 10.1007/s00542-007-0400-7

TECHNICAL PAPER

Post-buckling dynamic behavior of self-assembled 3D microstructures

Lionel Buchaillot · Olivier Millet · Emmanuel Quévy · Dominique Collard

Received: 10 October 2006 / Accepted: 9 February 2007 / Published online: 16 March 2007

Abstract The paper presents the snap-through phenomenon in the case of micro fabricated clamped-clamped buckled beam. This dynamic post-buckling behavior is likely to occur in 3D microstructures when they are subjected to large vibration amplitudes. The main difference between this work and previous studies is the MEMS specific beam dimension, especially the large initial deflection of the buckled beam that involves the inversion of the two first resonance frequencies. The mathematical development allows showing how the vibration amplitude of the supporting base affects the post-buckling dynamic behavior of the beam. For each frequency, the limit between the stable behavior and the snap-through behavior is evaluated. Moreover, the effect of environment is taken into account from the damping point of view. Samples are fabricated and the experiment is described. Measurements are compared to the theoretical approach and the results are in good agreement with the proposed model.

L. Buchaillot (✉) · O. Millet · E. Quévy
Institut d'Electronique et de
Micro-Electronique et de Nanotechnologie,
Dept. ISEN, Cité Scientifique,
IEMN, UMR CNRS 8520, Avenue Poincaré,
B.P. 60069, 59652 Villeneuve d'Ascq Cedex, France
e-mail: Lionel.Buchaillot@isen.iemn.univ-lille1.fr

D. Collard
LIMMS/IIS-CNRS,
Institute of Industrial Sciences,
The University of Tokyo, Tokyo, Japan

1 Introduction

When compared to a microelectronic device, a micro nano electro mechanical system (MEMS or NEMS) exhibits a major difference due to its ability to produce a displacement once it has been released from a substrate. However, for many years, the achievable vertical motion was determined by the thickness of the sacrificial layer which is typically in the range of 2 μm. Thus, for example, the resulting micro mirrors rotation excursion was only of a few degrees. In order to overcome this limitation, two solutions have been successfully implemented in the processes: on the one hand, it consists in the bulk etching of the substrate by different means (chemical etching or deep reactive ion etching); and on the other hand, the microstructure is first fabricated by surface micromachining and subsequently lifted up until the final shape is obtained. In the literature, the elevation of the device is obtained either by rotating the mobile parts around polycrystalline silicon hinges (Pister et al. 1992) or by bending of a thin polycrystalline silicon strips (Suzuki et al. 1994; Lin et al. 1997). Microrobots (Suzuki et al. 1994), a microprobe (Lin et al. 1997) and Micro-Opto-Electro-Mechanical Systems (MOEMS) (Wu et al. 1995; Tien et al. 1996) have been fabricated with such 3D techniques.

Nevertheless, micro manipulation involved in these folding steps is likely to cause irreversible damages to the microstructures. In order to comply with mass-production capability, a safe and automatic procedure is required. Such a self-assembly capability has been demonstrated already by using upward bending induced by electrochemical oxidation (Smela et al. 1995), Lorentz forces (Shimoyama et al. 1998), melting photoresist pads (Syms and Yeatman 1993), or polymer shrinkage process (Ebefors et al. 1998). Even if these techniques have been highly improved (Syms

2000a, b), most of them require a very precise monitoring of the assembly process aiming at the final shape control. To overcome this difficulty, latches have been implemented on self-assembled structures for MOEMS applications and presented in recent studies (Syms 1999; Syms et al. 2001).

With polycrystalline silicon micromachining and integrated electrostatic actuation, 3D self-assembly achieved through vertical buckling of micro-beams showed to be a very promising alternative approach (Fang and Wickert 1994; Garcia 1998; Akiyama et al. 1997). Scratch Drive Actuators (SDA) (Akiyama and Shono 1993) produce a force able to trigger buckling of a beam and the 3D shape is subsequently kept permanent by the so-called reshaping technology (Fukuta et al. 1997; Fan et al. 1997; Lee et al. 1997).

Self-assembly process is very attractive in the MOEMS field because it allows larger deflection amplitudes of micro-mirrors. Although being very attractive, the self-assembly process exhibits a major drawback that is the low stiffness in the vertical direction. Therefore, a bistable mechanical behavior can be expected if a static force is applied along the vertical axis of the micro structure, see figure 1. The static snap-through has been recently investigated in the MEMS's field by Jin et al. (2001) and Vangbo (Vangbo 1998; Vangbo and Bäcklund 1998). It consists in an instability allowing a mechanically bistable structure to switch between two states of equilibrium (Zycskowski 2005). In addition to static occurrences, snap-through can also be triggered by a dynamical action. In both case, it ends up in failure of the 3D device. In this paper the snap-through phenomenon has been studied in the case of 3D micro devices submitted to vibrations. The principal idea is to ensure a large number of operations and the understanding of the failure mechanisms. Over the past years, numerous works dealing with beam large amplitude vibration with fixed distance between supports during vibration have been reported. Humphreys (1966) examined a circular arch under impulse-step and rectangular pulse loading by using an analog computer. Lock (1966) determined the critical step-pressure loads of an arch by the numerical integration of the equations of motions and by an infinitesimal stability analysis. Mettler (1967) applied the method of averaging to investigate the stability and the vibration of a sine arch under harmonic excitation. Tseng and Dugundji (1970, 1971) include the dynamic overshoot effect due to transient response in order to investigate the snap-through problem. The main differences between this study and the previous studies are the parameters of the beam, especially the ratio a (initial deflection to the thickness of the buckled beam). In the previous studies, a is lower than 10, whereas in most of the MEMS devices, a is bigger than 100 implying the inversion of the first two modes. Moreover, using Nayfeh's algorithm, we have found an exact value of the resonant frequencies in the case of a buckled beam. Finally, we have studied the damping factor, which happened to be high due to the air viscosity.

The study presents the effect of the inversion of the two first modes on snap-through problem. Secondly, we determine the snap-through domain and parameters (stability's criteria, damping influence). Moreover, the eigen-frequencies of the first two modes in the case of a buckled beam are calculated by the Nayfeh's algorithm. Finally, the dynamic snap-through behavior is investigated. Both analytical and experimental work are considered here.

2 Modeling

2.1 Equations of motion

This part gives a mathematical description of the system in order to discover the criteria that influence snap-through phenomenon. This study deals with a buckled beam (the beam originally flat, which has been compressed beyond the critical buckling load P_{cr}) with fixed ends and excited by the base motion W_B (Fig. 1). The governing differential equation of such a buckled beam is

$$E \cdot I \frac{\partial^4}{\partial x^4}(W + W_0) - \frac{\partial}{\partial x}\left[N_x \frac{\partial}{\partial x}(W + W_0)\right] = -m \cdot \left(\frac{\partial^2 W}{\partial t^2} + \frac{\partial^2 W_B}{\partial t^2}\right) - c \cdot \frac{\partial W}{\partial t} \tag{1}$$

$$\text{Assuming :} \quad N_x = -P_0 + \frac{E \cdot A}{2 \cdot l} \int_0^l \left[\frac{\partial}{\partial x}(W + W_0(x))\right]^2 .dx \tag{2}$$

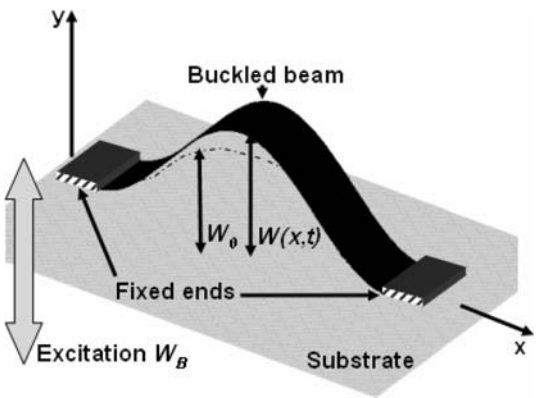

Fig. 1 Scheme of a buckled beam with fixed ends

W_B is the base displacement, W_0 is the initial static deflection and W is the beam displacement. The parameters which describe the structure are the moment of inertia I, the mass per unit of length m, the length l, the beam cross section A and the Young's modulus E. The other quantities are the time t, the damping coefficient c and N_x the total tension force on beam.

P_0 is a fictitious compressive force on the beam (3).

$$P_0 = P_{cr} + \frac{A \cdot E}{2l} \int_0^l \left(\frac{\partial W_0(x)}{\partial x} \right)^2 dx \tag{3}$$

P_{cr} is the fundamental buckling load of the clamped–clamped beam (4).

$$P_{cr} = \frac{4.\pi^2.E.I}{l^2} \tag{4}$$

The initial static deflection W_0 of the buckled beam is defined as follows (5).

$$W_0(x) = \frac{a \cdot h}{2}(1 - \cos\frac{2\pi x}{l}) \tag{5}$$

h is the beam thickness and $a = \frac{W_c}{h}$ with $W_c = W_0\left(\frac{l}{2}\right)$

a is a very important factor because it implies the inversion of the first two modes. Classical studies are based on a ratio a corresponding to a straight beam ($a < 10$), involving that the natural frequency of the first mode is linearly proportional to a, and that the natural frequency of the second mode is constant. In the case of the structure used in microactuators, the ratio a is bigger than 100 (experimentally $a = 200$). Therefore, new assumptions have to be stated. First, the natural frequency of the first mode is not considered proportional to a. Secondly, the natural frequency of the second mode is smaller than the natural frequency of the first mode, and the second mode is not constant.

Then, the inversion of the first two modes is done. The influence of the second mode on the first mode must be taken into account in the snap-through phenomenon. In order to study this inversion, the Simple Harmonic Motion (SHM) solutions and the Super Harmonic Motion (SPHM order 2, 3) solutions have to be determined.

2.2 Determination of SHM solutions and SPHM (order 2 and 3) solutions

Wah (1964) stated that a necessary but not sufficient condition for the existence of normal modes in nonlinear continuous system is that the space and time variables must be separable. The beam with fixed supports exhibits this character. Based on this property, a normal mode solution (6) is assumed.

$$W(x,t) = \sum_{n=1}^{2} \phi_n(x) \cdot \tilde{q}_n(t) \tag{6}$$

$\tilde{q}_1$ and $\tilde{q}_2$ are generalized coordinates. φ_1 and φ_2 are the first and second buckling modes, which must individually satisfy the geometric boundary conditions of the beam. Due to the clamped ends, the boundary conditions are $W = \frac{\partial W}{\partial x} = 0$ at $x = 0,l$; involving equations (7) and (8).

$$\phi_1 = \frac{a \cdot h}{2}(1 - \cos(2\pi\xi)) \tag{7}$$

$$\phi_2 = a \cdot h \cdot [\beta(j\xi - \sin(j\xi)) + \cos(j\xi) - 1] \tag{8}$$

where j = 8,986 (Tseng and Dugundji 1970, 1971), $\beta = \frac{2}{j}$ and $\xi = \frac{x}{l}$. Now, to find the SHM and SPHM solutions comes to determine the unknown coefficients $\tilde{q}_n(t)$. They are evaluated using Galerkin's method (Tseng and Dugundji 1970, 1971; Wah 1964; Min and Eisley 1972), which results in a set of nonlinear coupled ordinary differential equations. Assuming harmonic excitation of the base $\tilde{W}_B(t) = \tilde{W}_{B1}(t) = A_1 \cdot \sin(\omega_F \cdot t)$ (excites the first mode) or $\tilde{W}_B(t) = \tilde{W}_{B2}(t) = A_2 \cdot \sin(\omega_F \cdot t)$ (excitation of the second mode), Eqs. (9) and (10) are obtained.

$$\frac{d^2\tilde{q}_1}{dt^2} + \frac{c}{m} \cdot \frac{d\tilde{q}_1}{dt} + \omega_1^2\tilde{q}_1 + \frac{3}{2} \cdot \omega_1^2\tilde{q}_1^2 + \frac{1}{2} \cdot \omega_1^2\tilde{q}_1^3 + 2.263\omega_1^2(\tilde{q}_1 + 1)\tilde{q}_2^2 = \tilde{W}_{B1}(t) \tag{9}$$

$$\frac{d^2\tilde{q}_2}{dt^2} + \frac{c}{m} \cdot \frac{d\tilde{q}_2}{dt} + \omega_2^2\tilde{q}_2 + 1.259 \cdot a^2 \cdot \omega_2^2\tilde{q}_2^3 + 0.278 \cdot a^2 \cdot \omega_2^2(\tilde{q}_1^2 + 2 \cdot \tilde{q}_1)\tilde{q}_2 = \tilde{W}_{B2}(t) \tag{10}$$

where ω_1 and ω_2 are the natural frequencies of the first two modes; ω_F is the external excitation frequency; A_1 and A_2 are the vibration amplitudes of the supporting base.

Now let $\omega_F.t = v.\tau$ [v is any integer (Tseng and Dugundji 1970)], $\tilde{q}_1 = q_1 - 1$ and $\tilde{q}_2 = q_2$, then Eqs. (7) and (8) are obtained.

$$\frac{d^2q_1}{d\tau^2} + 2v\zeta_1\sqrt{\alpha_1} \cdot \frac{dq_1}{d\tau} + (v^2K_1 \cdot \alpha_1 + v^2K_4 \cdot \alpha_1 \cdot q_2^2).q_1 + v^2K_2 \cdot \alpha_1 \cdot q_1^3 = W_{B1}(\tau) \tag{11}$$

$$\frac{d^2q_2}{d\tau^2} + 2v\zeta_2\sqrt{\alpha_2} \cdot \frac{dq_2}{d\tau} + (v^2(K_5 - K_7 \cdot a^2) \cdot \alpha_2 + v^2 \cdot a^2 \cdot K_7 \cdot \alpha_2 \cdot q_1^2).q_2 + v^2K_6 \cdot \alpha_2 \cdot a^2 \cdot q_2^3 = W_{B2}(\tau) \tag{12}$$

$$K_1 = -0,5; \quad K_2 = 0,5; \quad K_4 = 2,263; \quad K_5 = 1;$$
$$K_6 = 1,258; \quad K_7 = 0,278$$
$$\alpha_1 = \left(\frac{\omega_1}{\omega_F}\right)^2 = \frac{1}{\Omega_1^2}; \quad \alpha_2 = \left(\frac{\omega_2}{\omega_F}\right)^2 = \frac{1}{\Omega_2^2};$$
$$\varsigma_1 = \frac{c}{2m\omega_1}; \quad \varsigma_2 = \frac{c}{2m\omega_2}.$$

At this level, the coefficients q_n (t) have to be evaluated in order to determine SHM and SPHM solutions. The present discussion has been restricted to the first two modes. Solving simultaneously Eqs. (11) and (12) turns out to be difficult. Therefore, the response is split into two cases: First mode Excited, Second mode at Rest (FESR), and Second mode Excited, First mode at Rest (SEFR).

Considering FESR case (W_{B2} (τ) = 0, q_2 = 0) and assuming W_{B1} $(\tau) = K_3 .A_{F1}\cdot\sin$ $(v .\tau)$, the governing equation for q_1 is obtained (13). In the same way, assuming W_{B2} $(\tau) = K_3 .A_{F2}\cdot\sin$ $(v .\tau)$ in the SEFR configuration (W_{B1} (τ) = 0, q_1 = 0), the governing equation (14) is obtained for q_2.

$$\frac{d^2q_1}{d\tau^2} + 2v\zeta_1\sqrt{\alpha_1}\cdot\frac{dq_1}{d\tau} + v^2K_1\cdot\alpha_1\cdot q_1 + v^2K_2\cdot\alpha_1\cdot q_1^3 = v^2\cdot K_3\cdot A_{F1}\cdot\sin(v\tau) \tag{13}$$

$$\frac{d^2q_2}{d\tau^2} + 2v\zeta_2\sqrt{\alpha_2}\cdot\frac{dq_2}{d\tau} + v^2(K_5 - K_7\cdot a^2)\cdot\alpha_2\cdot q_2 + v^2K_6\cdot\alpha_2\cdot a^2\cdot q_2^3 = v^2\cdot K_3\cdot A_{F2}\cdot\sin(v\tau) \tag{14}$$

$$K_3 = 1,333; \quad A_{F1} = \frac{A_1}{a.h}; \quad A_{F2} = \frac{A_2}{a.h}.$$

Next, considering that v = 1 (Tseng and Dugundji 1970), from normalized equations (13) and (14), it can be observed that the normalized vibrations amplitudes of the supporting base (A_{F1}, A_{F2}) and the damping coefficients (ζ_1, ζ_2) are the only external parameters governing the snap-through phenomenon. It can be deduced that the snap-through is a function of the damping and the vibrations amplitudes of the supporting base. In addition to the analysis of the inversion of the first two modes, the study of SHM and SPHM solutions show the influence of these two parameters on the snap-through.

The Eqs. (13) and (14) have the same form as Duffing's equation; except for K_1 (13) and (K_5–$K_7.a^2$) (14) that are negatives. So the general solution of equations (13) and (14) before snapping-through can be approximated (15), (16).

$$q_1 = y_{1,0} + \sum_{k=1}^{3}(x_{1,k}\cdot\sin(k\tau) + y_{1,k}\cdot\cos(k\tau)) \tag{15}$$

$$q_2 = y_{2,0} + \sum_{k=1}^{3}(x_{2,k}\cdot\sin(k\tau) + y_{2,k}\cdot\cos(k\tau)) \tag{16}$$

Substituting (15) into (13), and (16) into (14), and using the method of harmonic balance for the constant $y_{1,0}$, $y_{2,0}$ and the first three harmonics, two sets of seven nonlinear coupled algebraic equations are obtained. The damping case has been considered because the air viscosity can not be neglected: 3D microstructures are so small and thin that damping effects (air frictions) are very critical. For the sake of clarity, only the general expression of the two sets is showed (19). Hence, it is considered that Eqs. (13) and (14) have the same form as (17), and Eqs. (15) and (16) is like Eq. (18).

$$\frac{d^2q_n}{d\tau^2} + 2\zeta_n\sqrt{\alpha_n}\cdot\frac{dq_n}{d\tau} + K'\cdot\alpha_n\cdot q_n + K''\alpha_n q_n^3 = K'''\cdot A_{Fn}\cdot\sin\tau \tag{17}$$

$$q_n = y_{n,0} + \sum_{k=1}^{3}(x_{n,k}\cdot\sin(k\tau) + y_{n,k}\cdot\cos(k\tau)) \tag{18}$$

$$\left.\begin{array}{c} K'.y_{n,0}^2 + K''.y_{n,0}.A_0 = 0 \\ K'.y_{n,0}.x_{n,1} + K''.y_{n,0}.A_1 - x_{n,1} - 2.y_{n,1}.\xi_n.\sqrt{y_{n,0}} = K'''.A_{Fn} \\ K'.y_{n,0}.x_{n,2} + K''.y_{n,0}.A_2 - 4.x_{n,2} - 4.y_{n,2}.\xi_n.\sqrt{y_{n,0}} = 0 \\ K'.y_{n,0}.x_{n,3} + K''.y_{n,0}.A_3 - 9.x_{n,3} - 6.y_{n,3}.\xi_n.\sqrt{y_{n,0}} = 0 \\ K'.y_{n,0}.y_{n,1} + K''.y_{n,0}.A_4 - y_{n,1} + 2.x_{n,1}.\xi_n.\sqrt{y_{n,0}} = 0 \\ K'.y_{n,0}.y_{n,2} + K''.y_{n,0}.A_5 - 4.y_{n,2} + 4.x_{n,2}.\xi_n.\sqrt{y_{n,0}} = 0 \\ K'.y_{n,0}.y_{n,3} + K''.y_{n,0}.A_6 - 9.y_{n,3} + 6.x_{n,3}.\xi_n.\sqrt{y_{n,0}} = 0 \end{array}\right\} \tag{19}$$

A_1, A_2, A_3, A_4, A_5 and A_6 are functions given in the *Appendix*. In order to compute the two sets, the first and second natural frequencies of the buckled beam have to be known.

Using Nayfeh's algorithm (Syms 2000a, 2000b) a good estimation of the eigenfrequencies of the first and second mode has been obtained for a buckled beam. This new value depends both on the initial deflection and the parameters of the beam. The algorithm starts by determining the critical load and the normal mode which corresponds to the boundary conditions of a clamped-clamped beam. Then, the equations of motion dealing with the state of the beam make an homogeneous system of equations which defines an eigenvalues problem for the natural frequency. This system of equations describes the dynamic response of the initially deflected fixed-fixed beam. To find a unique non-zero solution, the determinant of the system must be zero. This conditions leads to the computation of the exact natural frequency.

Finally, the good assessment of the eigenfrequencies of the buckled beam leads to the solution of the two sets of equations found in both cases by using a Newton iteration method. It allows showing the exact solutions of SHM, and SPHM (order 2 and 3). As an example, the solution of $y_{1,1}$

is shown in Fig. 2; for this calculation, the normalized vibration amplitude A_{F1} of the supporting base is 0.3, and the non-damping case is considered.

2.3 Stability

The stability of the system is depends on the continuity of SHM solutions and SPHM (order 2 and 3) solutions. For each excitation frequency, the continuity of the previous solutions is analyzed. It is considered that the system is stable when SHM and SPHM solutions are continuous. So, for each frequency and for a fixed damping coefficient, the normalized vibrations amplitude of the supporting base is increased until the non-continuity of the solutions is reached. It allows to determine, for each frequency, the highest stable vibration amplitude of the supporting base. Beyond this limit, the system is inevitably instable.

The method has been applied in the previous cases. So, for each frequency, $A_{F1\ \max}$ is determined in the FESR case and $A_{F2\ \max}$ in the SEFR case. Concerning the general case (i.e., the first and the second mode excited at the same time), it is assumed that the highest vibration amplitude $A_{F\ \max}$ of the supporting base, within the stability region of the system, is equal to the minimum of ($A_{F1\ \max}$, $A_{F2\ \max}$).

2.4 Results

The major result is that $A_{F1\ \max} = A_{F\ \max}$ for each frequency (Fig. 3); it confirms that the second mode is stable. So, the inversion of mode does not influence the snap-through phenomenon. Moreover, from the previous stability analysis, one can find two stable steady-state solutions for the buckled beam in the non-damping case at frequencies lower than $\Omega_1 = \frac{1}{k}$, where k = 1,2,3. The snapping phenomenon generally occurs near jump points (k = 1,2,3). A non-zero damping coefficient implies a bigger stability state, i.e., any jump point (k = 2,3) has been observed (Fig. 3). So, the vibration amplitude of the supporting base is the stability criterion for the snap-through and damping prevents snap-through phenomenon from occurring.

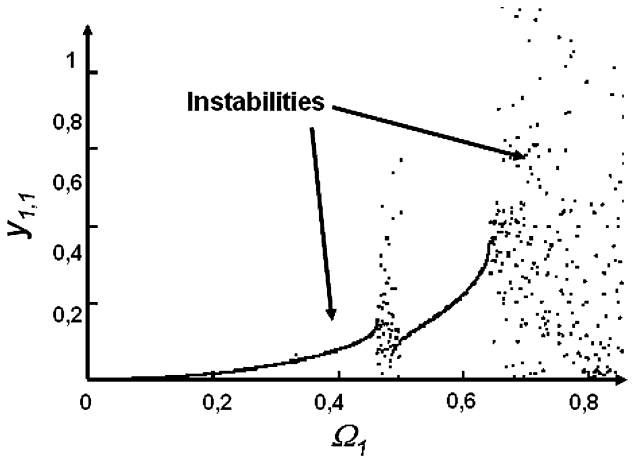

Fig. 2 Dynamical behavior of $y_{1,1}$ with intermittent instabilities. For this calculation, the normalized vibration amplitude A_{F1} of the supporting base is 0.3, and the non-damping case is considered

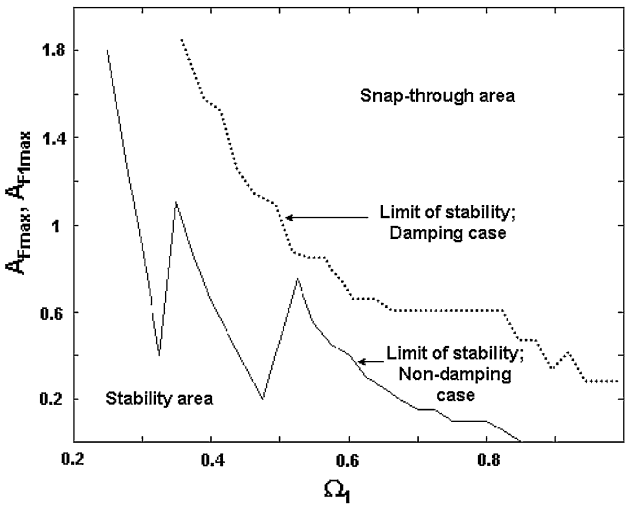

Fig. 3 Snap-through regions and limits of stability. The major result is that $A_{F1\ \max} = A_{F\ \max}$ for each frequency; it confirms that the second mode is stable. Two stable steady-state solutions are found for the buckled beam in the non-damping case at frequencies lower than $\Omega_1 = \frac{1}{k}$, where k = 1,2,3. A non-zero damping coefficient implies a bigger stability state, i.e., any jump point (k = 2,3) has been observed

2.5 Dynamic response using Runge–Kutta method

In order to validate the previous model, numerical simulations have been performed. Considering the transient response, the snapping phenomenon has been solved directly by numerical methods. Accordingly, the Runge–Kutta numerical integration method has been employed using different time increment. The calculations were performed at the vicinity of jump points. The initial conditions, which correspond to the beam at rest, were employed (20); the second mode is considered at rest because the previous results confirm the second mode stability.

$$q_1 = 1, \quad \frac{dq_1}{d\tau} = 0, \quad q_2 = 0 \ \text{ and } \ \frac{dq_2}{d\tau} = 0 \ \text{ at } \ \tau = 0. \tag{20}$$

Some typical dynamic behaviors are shown in Fig. 4. At a fixed excitation frequency, if the supporting base amplitude is higher than $A_{F\ \max}$, it can be observed that the snap-through problem begins and the buckled beam vibration amplitude becomes large (Fig. 4). Moreover, with the same set of parameters, if the damping effects get bigger,

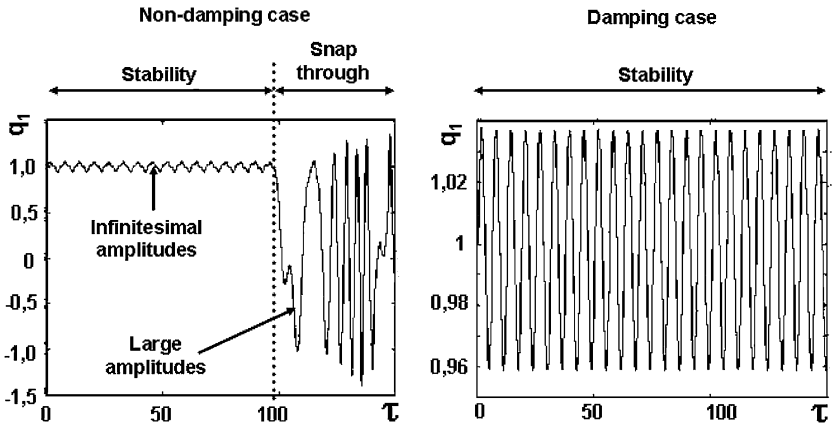

Fig. 4 Influence of damping on dynamic SHM snap-through. At a fixed excitation frequency, if the supporting base amplitude is higher than $A_{F\ max}$, it can be observed that the snap-through problem begins and the buckled beam vibration amplitude becomes large. Moreover, with the same set of parameters, if the damping effects get bigger, snap-through can be avoided resulting in a stable dynamic behavior

snap-through can be avoided resulting in a stable dynamic behavior (Fig. 4).

2.6 Application

In order to demonstrate how useful the modeling is, the following example is given. MEMS device consists in a deformable plate which is fixed to buckled beams (Akiyama et al. 1997; Quévy et al. 2000). This type of device is used to actuate a continuous-membrane for adaptive optics application. Such an optical MEMS is supposed to be part of a space laboratory subjected to a dynamical excitation during the launcher lift-off.

3 Experiment

3.1 Technological process

In order to validate the modeling, samples have been fabricated. The 3D structure is obtained thanks to SDAs coupled to a slender beam the length, width and thickness of which are 550, 8 and 0.48μm, respectively (Akiyama et al. 1997; Quévy et al. 2000). The process flow of a SDA and a contact pad is shown in Fig. 5. Starting with a 5–20 ohm cm, p-type (100) wafer, a 0.35μm oxide is grown, followed by the first Low Pressure Chemical Vapor Deposition (LPCVD) polycrystalline silicon layer. After the electrode patterning, the polycrystalline silicon is oxidized and covered by a LPCVD silicon nitride (Si_3N_4) layer (Fig. 5a). 2μm sacrificial oxide (SiO_2) has been deposited followed by the etching of SDA bushing and contact pad (Fig. 5b). 2μm LPCVD polycrystalline silicon was deposited, doped by phosphorus implantation and annealed at 1,000°C for 60 min (Fig. 5c) for the dopant diffusion. The structural patterned has been defined by SF_6 and Cl_2 etching. The polycrystalline silicon was then thinned down to 0.5μm by SF_6 plasma. Finally, the structure has been released in HF (Fig. 5d).

3.2 Lifting-up the beam

SDAs make supporting beams buckling resulting in the beam lift-up (initial deflection: 97μm), until the SDA mobile part is latched and locked to mechanical anchors (Fig. 6) (Syms and Yeatman 1993). This locking technique avoids the use of reshaping and thus enables good prediction of the buckled beam shape. The buckled beam is rigidly clamped at both ends by the use of mechanical anchors. A SEM observation allows to check the symmetrical shape of the deformed beam (Fig. 6).

3.3 Measurements

3.3.1 Natural frequencies of the first two modes

The wafer was glued onto a piezoelectric ceramic. The excitation of the piezoceramic (therefore the wafer) is controlled by a network analyzer. An Optical Beam Deflection (OBD) method (Fig. 7) (Buchaillot et al. 1997) is used to determine the exact value of natural frequency of the first two modes. OBD is a well-known nondestructive optical method: a laser beam is focused on the sample by means of a microscope objective. The reflected beam reaches the four-quadrant photodiode used as a vibration detector. The photodiode's signal is compared to the excitation frequency leading to the exact value of the first and second natural frequency of the microstructure, thus validating the theoretical approach.

3.3.2 Snap-through

The goal of this experiment was to verify that, at a fixed excitation frequency, for two different values of the vibration amplitude of the supporting base (one lower than

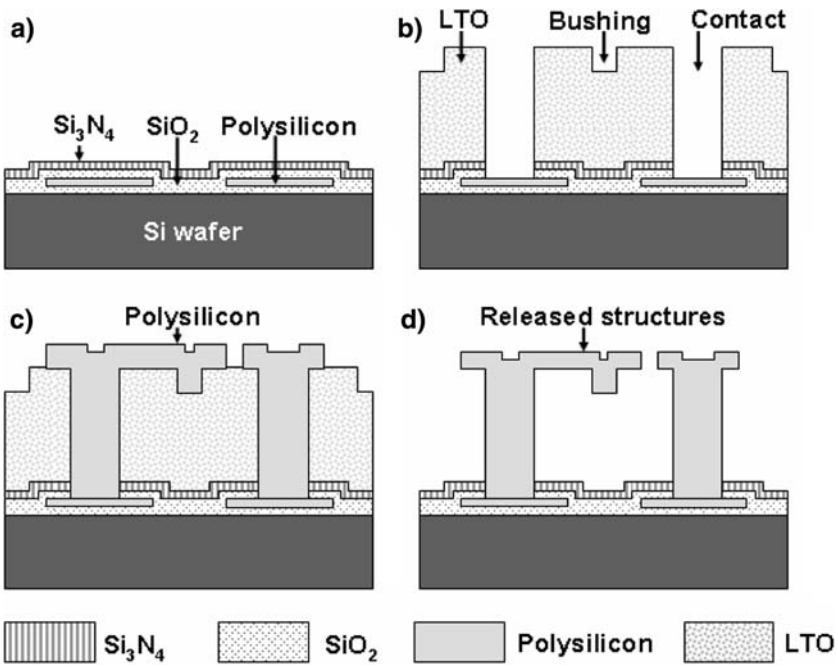

Fig. 5 Simplified process flow representing surface micromachining of two polycrystalline silicon layers

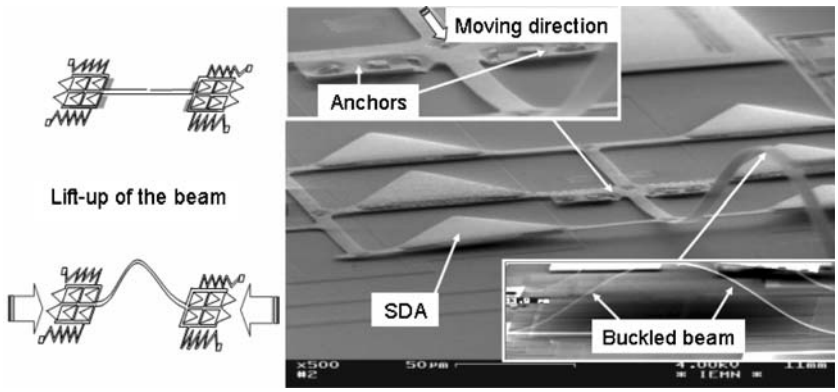

Fig. 6 Scanning electron microscope image of a buckling beam with its anchors. SDA are also visible

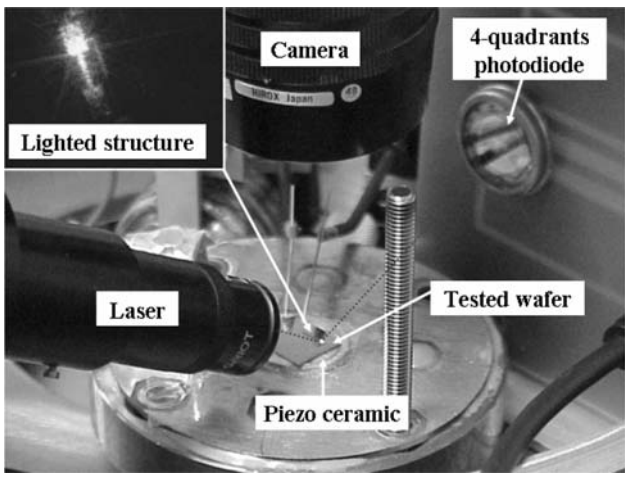

Fig. 7 Optical beam deflection experimental set-up for the detection of resonance frequencies (This test bench is in a vacuum chamber)

the determined limit of stability—Fig. 3—and the other one upper than the limit of stability), two different dynamical behaviors (stability, snap-through phenomenon) are observed. So, the test bench is under vacuum In order to consider the damping equal to zero, a vacuum chamber was used. The test is performed at a fixed excitation frequency equal to half of the first natural frequency of the buckled beam (22 kHz, obtained from Nayfeh's algorithm).The dynamical response at a jump point is investigated in order to reach rapidly the instability (Fig. 3). At this frequency, in the case of our structure (initial deflection of 97 μm), the modeling predicts a limit of stability corresponding to a 19.4 μm vibration amplitude for the supporting base equal. First, the vibration amplitude of the supporting base is set to 10 μm (via the voltage control of the piezoceramic). Secondly, the amplitude of the base is set to 25–30 μm. The snap-through domain is determined for SHM. The OBD method is used for the determination of the vibration amplitude of the buckled beam, and the four-quadrant

photodiode is used as a position sensitive detector (PSD). The output signal of the PSD has been analyzed by a scope; the voltage observed is proportional to the vibration amplitude of the buckled beam.

3.4 Results

3.4.1 Natural frequencies of the first two modes

Given that the initial post-buckling deflection is available, the Nayfeh's algorithm predicts the resonance frequencies (ω_1, ω_2) and the mode inversion ($\omega_1 > \omega_2$). The initial deflection was the only experimental parameter used as an input for the computation. Figure 8 shows the experimental values of the resonance frequencies for the modes of the base and of the buckled beam. Table 1 presents a comparison between the experimental and the theoretical results. For the first resonant mode, the difference between experimental values and the values predicted by the theory is low. The explanation is twofold: First, in our case, the buckled beam has been assumed to exhibit the ideal fixed-end boundary conditions usually met in structures at the macroscale. In the real structure, the buckled beam boundary conditions are found to better correspond to elastically constraints against rotation ends that differs from the theoretical fixed-end boundary conditions. Secondly, stress failure may appear in the beam after releasing of the structure.

3.4.2 Snap-through

The stability is confirmed by the analog computer solutions when the vibration amplitude of the supporting base is lower than the limit of stability (19.4 μm): the steady-state SHM shows infinitesimal amplitudes. Figure 9 shows the results for the same buckled beam, at the same frequency, but with vibration amplitude of the base equal to 25–30 μm. The transition to the snap-through behavior is obvious. Very large amplitudes are obtained, thus validating the modeling.

4 Conclusion

Snap-through phenomenon has been considered in the case of microfabricated clamped–clamped buckled beam. The main differences between this study and the previous study are the MEMS specific beam parameters, especially the initial deflection of the buckled beam. In the MEMS field, the ratio a is higher than 100 (in experiment, $a = 200$) involving the inversion of the two first resonance frequencies. Some conclusions have been drawn: First, the vibration amplitude of the supporting base appears to be the triggering factor for snap-through phenomenon. For each frequency, the limit between the stable behavior and the snap-through behavior has been evaluated. Secondly, the second mode is stable meaning that the instability is confirmed with only the first mode. Moreover, it has been shown that damping tempers the snap-through phenomenon by increasing the stable state of the system. Finally, the experimental results of the natural frequencies of the first two modes are in good agreement with the theoretical results. The present study has demonstrated the importance of dynamical snap-through in the understanding of the vibration behaviour of microfabricated buckled beams.

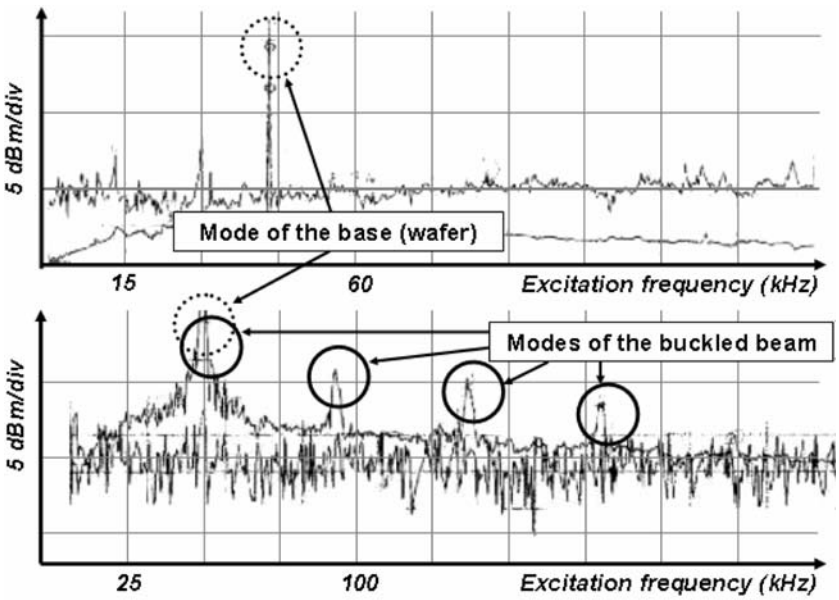

Fig. 8 Frequency response measured for the buckled beam on the substrate (at atmospheric pressure)

Table 1 Comparison between experimental and theoretical data for the first and the second resonant modes

Beam dimensions		
Length: 550 μm	Experimental results	Theoretical results
Width: 8 μm	Mode2: 29,705 Hz	Mode2: 29,501 Hz
Thickness: 0.477 μm	Mode1: 42,811 Hz	Mode1: 44,201 Hz
Initial deflection: 97 μm		

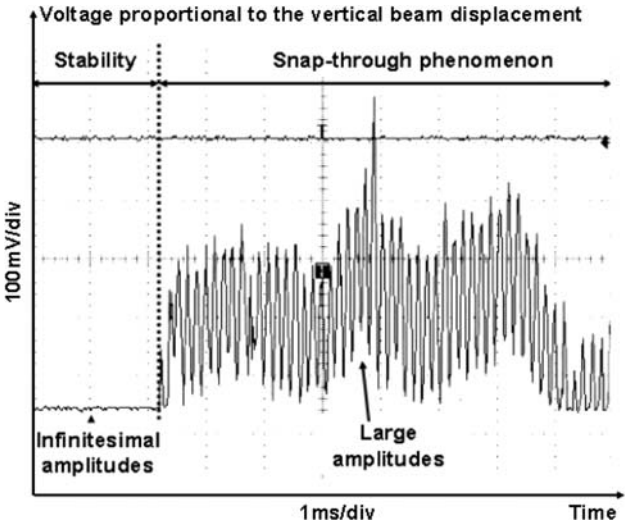

Fig. 9 Experimental results showing the snap-through occurrences

5 Appendix

$$A_0 = (1,5.x_{n,1}.x_{n,2}.y_{n,1} + 1,5.x_{n,2}.x_{n,3}.y_{n,1} - 0,75.x_{n,1}^2.y_{n,2} + 1,5.x_{n,1}.x_{n,3}.y_{n,2} - 1,5.x_{n,1}.x_{n,2}.y_{n,3} + y_0^3 + 1,5.y_{n,0}.x_{n,1}^2 + 1,5.y_{n,0}.x_{n,2}^2 + 1,5.y_{n,0}.x_{n,3}^2 + 1,5.y_{n,0}.y_{n,1}^2 + 1,5.y_{n,0}.y_{n,2}^2 + 1,5.y_{n,0}.y_{n,3}^2 + 0,75.y_1^{n,2}.y_{n,2} + 1,5.y_{n,1}.y_{n,2}.y_{n,3})$$

$$A_1 = (3.y_{n,0}.x_{n,2}.y_{n,1} - 3.y_{n,0}.x_{n,1}.y_{n,2} + 3.y_{n,0}.x_{n,3}.y_{n,2} - 3.y_{n,0}.x_{n,2}.y_{n,3} + 3.y_{n,0}^2.x_{n,1} + 0,75.x_{n,1}^3 - 0,75.x_{n,1}^2.x_{n,3} + 1,5.x_{n,1}.x_{n,2}^2 + 1,5.x_{n,1}.x_{n,3}^2 + 0,75.x_{n,2}^2.x_{n,3} + 0,75.x_{n,1}.y_{n,1}^2 + 1,5.x_{n,1}.y_{n,2}^2 - 1,5.x_{n,1}.y_n,1.y_{n,3} + 1,5.x_{n,1}.y_{n,3}^2 + 1,5.x_{n,2}.y_{n,2}.y_{n,3} - 0,75.x_{n,3}.y_{n,2}^2 + 0,75.x_{n,3}.y_{n,1}^2)$$

$$A_2 = (3.y_{n,0}.x_{n,1}.y_{n,1} + 3.y_{n,0}.x_{n,3}.y_{n,1} - 3.y_{n,0}.x_{n,1}.y_{n,3} + 3.y_{n,0}^2.x_{n,2} + 1,5.x_{n,1}^2.x_{n,2} + 1,5.x_{n,1}.x_{n,2}.x_{n,3} + 0,75.x_{n,2}^3 + 1,5.x_{n,2}.x_{n,3}^2 + 1,5.x_{n,1}.y_{n,2}.y_{n,3} + 0,75.x_{n,2}.y_{n,2}^2 - 1,5.x_{n,2}.y_{n,1}.y_{n,3} + 1,5.x_{n,2}.y_{n,3}^2 + 1,5.x_{n,3}.y_{n,1}.y_{n,2} + 1,5.x_{n,2}.y_{n,1}^2)$$

$$A_3 = (3.y_{n,0}.x_{n,2}.y_{n,1} + 3.y_{n,0}.x_{n,1}.y_{n,2} - 0,25.x_{n,1}^3 + 3.y_{n,0}^2.x_3 + 1,5.x_{n,1}^2.x_{n,3} + 0,75.x_{n,1}.x_{n,2}^2 + 1,5.x_{n,2}^2.x_{n,3} + 0,75.x_3^3 + 0,75.x_{n,1}.y_{n,1}^2 - 0,75.x_{n,1}.y_{n,2}^2 + 1,5.x_{n,3}.y_{n,1}^2 + 1,5.x_{n,2}.y_{n,1}.y_{n,2} + 1,5.x_{n,3}.y_{n,2}^2 + 0,75.x_{n,3}.y_{n,3}^2)$$

$$A_4 = (3.y_{n,0}^2.y_{n,1} + 0,75.x_{n,1}^2.y_{n,1} + 1,5.x_{n,1}.x_{n,3}.y_{n,1} + 1,5.x_{n,2}^2.y_{n,1} + 1,5.x_{n,3}^2.y_{n,1} + 1,5.x_{n,2}.x_{n,3}.y_{n,2} - 0,75.x_{n,1}^2.y_{n,3} - 0,75.x_{n,2}^2.y_{n,3} + 3.y_{n,0}.x_{n,1}.x_{n,2} + 3.y_{n,0}.x_{n,2}.x_{n,3} + 3.y_{n,0}.y_{n,2}.y_{n,3} + 0,75.y_{n,1}^3 + 1,5.y_{n,1}.y_{n,2}^2 + 0,75.y_{n,1}^2.y_{n,3} + 0,75.y_{n,2}^2.y_{n,3} + 1,5.y_{n,1}.y_{n,3}^2 + 3.y_{n,0}.y_{n,1}.y_{n,2})$$

$$A_5 = (1,5.x_{n,2}.x_{n,3}.y_{n,1} + 3.y_{n,0}^2.y_2 + 1,5.x_{n,1}^2.y_{n,2} - 1,5.x_{n,1}.x_{n,3}.y_{n,2} + 0,75.x_{n,2}^2.y_{n,2} + 1,5.x_{n,3}^2.y_{n,2} + 1,5.x_{n,1}.x_{n,2}.y_{n,3} - 1,5.y_{n,0}.x_{n,1}^2 + 3.y_{n,0}.x_{n,1}.x_{n,3} + 1,5.y_{n,0}.y_{n,1}^2 + 3.y_{n,0}.y_{n,1}.y_{n,3} + 1,5.y_{n,1}^2.y_{n,2} + 1,5.y_{n,1}.y_{n,2}.y_{n,3} + 0,75.y_{n,2}^3 + 1,5.y_{n,2}.y_{n,3}^2)$$

$$A_6 = (-0,75.x_{n,1}^2.y_{n,1} - 0,75.x_{n,2}^2.y_{n,1} + 3.y_{n,0}^2.y_{n,3} + 1,5.x_{n,1}.x_{n,2}.y_{n,2} + 1,5.x_{n,1}^2.y_{n,3} + 1,5.x_{n,2}^2.y_{n,3} + 0,75.x_{n,3}^2.y_{n,3} - 3.y_{n,0}.x_{n,1}.x_{n,2} + 3.y_{n,0}.y_{n,1}.y_{n,2} + 0,25.y_{n,1}^3 + 0,75.y_{n,1}.y_{n,2}^2 + 1,5.y_{n,1}^2.y_{n,3} + 1,5.y_{n,2}^2.y_{n,3} + 0,75.y_{n,3}^3)$$

References

Akiyama T, Shono K (1993) Controlled stepwise motion in polysilicon structures. J Microelectromechan Syst 2:106–110

Akiyama T, Collard D, Fujita H (1997) Scratch-drive Actuator with mechanical link for self-assembling of three-dimensional MEMS. J Microelectromech Syst 6:10–17

Buchaillot L, Farnault E, Hoummady M, Fujita H (1997) Silicon nitride thin films Young's modulus determination by an optical non destructive method. Jpn J Appl Phys 36:L794–L797

Ebefors T, Kälvesten E, Stemme G (1998) New small radius joints based on thermal shrinkage of polyimide in V-grooves for robust self-assembly of 3D microstructures. J Micromech Microeng 8:188–194

Fan L, Wu MC, Choquette KD, Crawford MH (1997) Self-assembled microactuated XYZ stage for optical scanning and alignment. In: Proceedings of 9th international conference on solid-state sensors and actuators (Transducer'97), Chicago, June 16–19, pp 319–322

Fang W, Wickert JA (1994) Postbuckling of micromachined beams. In: Proceedings of IEEE workshop on micro electro mechanical system, Oiso, pp 182–187

Fukuta Y, Collard D, Akiyama T, Yang EH, Fujita H (1997) Microactuated self-assembling of 3D polysilicon structures with reshaping technology. In: Proceedings of 10th international workshop on micro electro mechanical system, Nagoya, pp 447–481

Garcia EJ (1998) Microflex mirror and instability actuation technique. In: Proceedings of 11th international workshop on micro electro mechanical system, Heidelberg, pp 470–475

Humphreys JS (1966) Dynamic snap buckling of shallow arches. AIAA J 4:878–886

Jin Q, Lang JH, Slocum AH (2001) A centrally-clamped Parallel-Beam Bistable MEMS mechanism. In: Proceedings of 11th international workshop on micro electro mechanical system, Heidelberg, pp 353–356

Lee SS, Motamedi E, Wu MC (1997) Surface micromachined free-space optic switches with integrated microactuators for optical fiber communication systems. In: Proceedings of 9th international conference on solid-state sensors and actuators (Transducer'97), Chicago, June 16–19, pp 85–88

Lin G, Palmer RE, K.Pister JS, Roos KP (1997) Single heart cell force measured in standard CMOS. In: Proceedings of 9th international conference on solid-state sensors and actuators. (Transducer'97), Chicago, June 16–19, pp 199–200

Lock MH (1966) Snapping of a shallow sinusoidal arch under a step pressure load. AIAA J 4(7):1249–1256

Mettler E (1967) Stability and vibration problems of mechanical systems under harmonic excitation. Dynamic stability of structures international conference, North Western University, Evanston, Oct. 1965. Pergamon Press, New York, pp 169–188

Min G-B, Eisley JG (1972) Nonlinear vibrations of buckled beams. J Eng Ind 94:637–646

Pister KS, Judy MW, Burger SR, Fearing RS (1992) Microfabricated hinges. Sens Actuators A 33:249–256

Quévy E, Buchaillot L, Bigotte P, Collard D (2000) 3D self-assembling and actuation of electrostatic micro-mirrors. ESSD-ERC 2000, pp 412–415

Shimoyama I, Kano O, Miura H (1998) 3D microstructures folded by Lorentz forces. In: Proceedings of 11th international workshop on micro electro mechanical system, Heidelberg, Jan 24–29, pp 25–29

Smela E, Inganä O, Lundströ I (1995) Controlled folding of micrometer-size structures. Science 268:1735–1738

Suzuki K, Shimoyama I, Miura H (1994) Insect model based microrobot with elastic hinges. J Microelectromech Syst 3:4–9

Syms RRA (1999) Surface tension powered self-assembly of 3D micro-optomechanical structures. J Microelectromech Syst 8:448–455

Syms RRA (2000a) Refractive collimating microlens arrays by surface tension self-assembly. IEEE Photon Tech Lett 12:1507–1509

Syms RRA (2000b) Self-assembled 3D silicon microscanners with self-assembled electrostatic drives. IEEE Photon Tech Lett 12:1519–1521

Syms RRA, Yeatman EY (1993) Self-assembly of fully three-dimensional microstructures using rotation by surface tension forces. Electron Lett 29:662–664

Syms RRA, Gormley C, Blackstone S (2001) Improving yield, accuracy an complexity in surface tension self-assembled MOEMS. Sens Actuators A 88(3):273–283

Tien NC, Solgaard O, Kiang MH, Daneman NJ, Lau KY, Muller RS (1996) Surface micromachined mirrors for laser beam positioning. Sens Actuators A 52:76–80

Tseng W-Y, Dugundji J (1970) Nonlinear vibrations of a buckled beam under harmonic excitation. J Appl Mech Trans ASME 37(2):292–297

Tseng W-Y, Dugundji J (1971) Nonlinear vibrations of a buckled beam under harmonic excitation. J Appl Mech 38:467–476

Vangbo M (1998) An analytical analysis of a compressed bistable buckled beam. Sens Actuators A 69:212–216

Vangbo M, Bäcklund Y (1998) A lateral symmetrically bistable buckled beam. J Micromech Microeng 8:29–32

Wah T (1964) The Normal Modes of Vibration of Certain Nonlinear Continuous Systems. Journal of Applied Mechanics, vol.31, Trans ASME, vol.86, No. 1, Mar. 1964, pp. 139–140

Wu MC, Lin LY, Lee SS, Pister KSJ (1995) Microfabricated free space integrated micro-optics. Sens Actuators A 50:127–134

Zycskowski M (2005) Post-buckling analysis of non-prismatic columns under general behaviour of loading. Int J Non-Linear Mech 40:445–463